THE JOURNAL OF PHYSICAL CHEMISTRY A

ARTICLE

pubs.acs.org/JPCA

Multipath Variational Transition State Theory: Rate Constant of the 1,4-Hydrogen Shift Isomerization of the 2-Cyclohexylethyl Radical

Tao Yu, Jingjing Zheng, and Donald G. Truhlar*

Department of Chemistry and Supercomputing Institute, University of Minnesota, Minneapolis, Minnesota 55455-0431, United States

ABSTRACT: We propose a new formulation of variational transition state theory called multipath variational transition state theory (MP-VTST). We employ this new formulation to calculate the forward and reverse thermal rate constant of the 1,4-hydrogen shift isomerization of the 2-cyclohexylethyl radical in the gas phase. First, we find and optimize all the local-minimum-energy structures of the reaction, product, and transition state. Then, for the lowest-energy transition state structures, we calculate the reaction path by using multiconfiguration Shepard interpolation (MSCI) method to represent the potential energy surface, and, from this representation, we also calculate the ground-state vibrationally adiabatic potential energy curve, the reaction-path curvature vector, and the generalized free energy of activation profile. With this information, the path-averaged generalized transmission coefficients $\langle\gamma\rangle$ are evaluated. Then, thermal rate constant containing the multiple-structure anharmonicity and torsional anharmonicity effects is calculated using multistructural transition state theory (MS-TST). The final MP-VTST thermal rate constant is obtained by multiplying $k_{\text{MS-T}}^{\text{MS-TST}}$ by $\langle\gamma\rangle$. In these calculations, the M06 density functional is utilized to compute the energy, gradient, and Hessian at the Shepard points, and the M06-2X density functional is used to obtain the structures (conformers) of the reactant, product, and the saddle point for computing the multistructural anharmonicity factors.

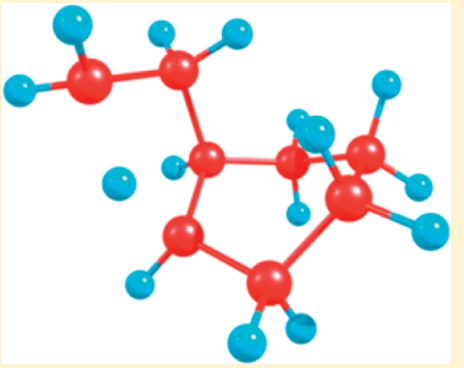

1. INTRODUCTION

The 1,4-hydrogen shift isomerization of an alkyl radical is an important type of reaction in combustion. The 1,4-hydrogen shift isomerizations of 1-pentyl[1−4] and 1-hexyl[3] radicals in the gas phase have been studied by both experimental and computational methods. In the present work, we calculate the thermal rate constant of another 1,4-hydrogen shift isomerization, in particular, that of a more complicated molecule, 2-cyclohexylethyl radical. The 2-cyclohexylethyl radical contains a six-membered ring and a side chain that has internal rotations around two carbon−carbon bonds, and these features require including torsional anharmonicity and a large number of diverse structures to model the reaction; this makes accurate calculation of the thermal rate constant challenging. In addition, the large size of the molecule makes minimum-energy-path[5] (MEP) calculations using direct-dynamics[6,7] algorithms very time-consuming.

In the present work, to address these issues and to compute the thermal rate constants for both the forward and reverse reactions efficiently, we propose a new formulation of variational transition state theory (VTST) called multipath VTST (MP-VTST); this formulation is based on the recent formulation[8] of multistructural VTST (MS-VTST). In MS-VTST, we employ only one reaction path to evaluate the dynamic recrossing and tunneling effects in the reaction. However, MP-VTST can be based on all reaction paths (full multipath) or a subset of dominating paths to calculate the quantum mechanical dynamic effects on reaction-coordinate motion. The potential energy surface in the broad vicinity of each reaction path is obtained by the multiconfiguration Shepard interpolation[9,10] (MCSI) method.

A key component of the free energy of reaction and free energy of activation for complex reactions is the conformational free energy, which is defined as the difference between the conformational−rotational−vibrational free energy calculated including all the conformations (also called structures) and that calculated including just the lowest-energy conformation. The free energy of activation includes the conformational free energy of the transition state minus that of reactants. MP-VTST, like MS-VTST, contains conformational free energy contributions based on the MS-T method[11] for including multiple-structure effects and explicit torsional anharmonicity in the partition functions of the reactant and saddle point configurations; thus it provides more reliable results than those calculated using single-structural variational transition state theory[12,13] (SS-VTST) with the harmonic approximation, especially at high temperature. In the present article, we also calculate reverse reaction rates, and therefore, we also calculate the conformational free energy and torsional anharmonicity of the product.

The MCSI method avoids the very expensive straight direct-dynamics method to obtain the MEP and ground-state vibrationally adiabatic potential curve V_a^G, and in particular, it efficiently generates a semiglobal potential energy surface based on a small number of high-level electronic structure calculations. In this article, the M06 density functional[14] is used to compute the energies, gradients, and Hessians of stationary Shepard points

Received: September 22, 2011
Revised: November 19, 2011
Published: November 29, 2011

(reactant well, product well, and saddle point) and nonstationary Shepard points along each reaction path. The Shepard-interpolated potential energy surface is used to compute the transmission coefficient for each reaction path by utilizing the multidimensional small-curvature tunneling (SCT) approximation.[13,15]

To obtain the MP-VTST rate constant, the multistructural anharmonicity factors are calculated by using the multistructural (MS) anharmonicity method[11,16] for the conformational−rotational−vibrational partition functions of the reactant, product, and transition state. For this purpose, we include all structures of the reactant, product, and saddle point, and we employ the M06-2X density functional[14] to obtain the structures of the reactant, product, and transition state, which are generated either by internal rotations around the carbon−carbon bond or by pseudorotation of the six-membered ring structure.

The theory presented here assumes that the internal states of the reactant, product, and transition state are described by a canonical ensemble. For a unimolecular reaction, this is called the high-pressure limit. For a bimolecular reaction, the theory assumes that the reaction is slow enough that energy transfer collisions maintain the reactant in a Boltzmann distribution.

2. METHODS

2.1. Electronic Structure Calculations. The M06-2X density functional[14] with the 6-311+G(2df,2p) basis set[17] was applied to optimize the geometries and obtain the frequencies for all the conformers of the reactant 2-cyclohexylethyl radical, the product *R*-2-ethylcyclohexan-1-yl radical, and the transition state. The 6-311+G(2df,2p) basis set for H and C is also called MG3S,[18] and we will use the short name for brevity.

For the global minimum-energy conformers of the reactant 2-cyclohexylethyl radical, the product *R*-2-ethylcyclohexan-1-yl radical, and the transition state, we employed the M06, M06-2X, and M08-SO[19] density functionals to optimize the geometries and calculate the energetics, in particular, the reaction energies and barrier heights. In addition, two multilevel methods, BMC-CCSD[20] and MCG3-TS,[21] and the ab initio CCSD(T)-F12a[22,23] method were used to calculate single-point energies at the M06-2X optimized geometries.

Other basis sets were also used for electronic structure calculations, including 6-31+G(d,p),[24] maug-cc-pVTZ,[25] aug-cc-pVTZ,[26] may-cc-pVTZ,[27] and def2-TZVP.[28] The M06 and M06-2X density functional calculations were performed by using the Gaussian 09 program,[29] the M08-SO density functional calculations were carried out via MN-GFM-4.1,[30] which is a locally modified version of Gaussian 03; CCSD(T)-F12a calculations were performed using Molpro;[31] and the BMC-CCSD and MCG3-TS calculations were carried out using MLGAUSS2.0.[32] The integration grid employed for density functional calculations of frequencies had 99 radial shells and 974 angular points per shell. The frequencies used for the partition function and multistructural torsional anharmonicity factor calculations in section 2.2 are obtained by using M06-2X/MG3S density functional calculations and multiplying the directly calculated values by an empirical frequency scaling factor[33] of 0.970.

2.2. Conformational−Vibrational−Rotational Partition Functions and Multistructural Torsional Anharmonicity Calculations. The complete conformational−rotational−vibrational partition functions of the reactant (R), product (P), and transition state (TS or ‡) were calculated by the MS method[15] mentioned above by using the MSTor program.[16] Including multiple structures and making the harmonic approximation in the vicinity of each local minimum of the potential energy surface is called the local harmonic (LH) approximation, and calculations including torsional anharmonicity have a suffix, -T. If one uses all structures (AS), one may call the resulting multistructural methods, MS-AS-LH and MS-AS-T. However, in the rest of this paper (and in future work, except when we need to emphasize that all structures are included), we will shorten MS-AS-LH and MS-AS-T to MS-LH and MS-T, respectively; this will not cause confusion in the present paper because we always employ all structures in the present article. (MS-AS-T and MS-AS-LH were called MS-AS and MS-HO, respectively, in the original[11] reference, but we have abandoned that notation as being too easily misunderstood.)

In the MS-LH and MS-T versions of the MS method, we, respectively, have

$$Q^{\text{MS-LH, X}}_{\text{con-rovib}} = \sum_{j=1}^{J} Q_{\text{rot},j} \exp(-\beta U_j) Q^{\text{HO}}_j \quad (1)$$

and

$$Q^{\text{MS-T, X}}_{\text{con-rovib}} = \sum_{j=1}^{J} Q_{\text{rot},j} \exp(-\beta U_j) Q^{\text{HO}}_j Z_j \prod_{\tau=1}^{t} f_{j,\tau} \quad (2)$$

where "con" denotes conformational, "rovib" denotes rotational−vibrational, and X can be R, P, or ‡, representing the reactant, product, and transition state; $Q_{\text{rot},j}$ is the classical rotational partition function of structure j, Q^{HO}_j is the normal-mode harmonic-oscillator vibrational partition function calculated at structure j, Z_j is a factor designed to ensure that the MS-T scheme reaches the correct high-T limit (within the parameters of the model), and $f_{j,\tau}$ is an internal-coordinate torsional anharmonicity function that, in conjunction with Z_j, adjusts the harmonic partition function of structure j for the presence of the torsional motion τ. As mentioned in section 2.1, frequencies used for the Q^{HO}_j, Z_j, and $f_{j,\tau}$ calculations were scaled by an empirical frequency scaling factor.[33] We use the label MS-LH to denote the partition function calculated without Z_j and $f_{j,\tau}$, that is, with all Z_j and all $f_{j,\tau}$ equal to unity.

When using either the MS-LH or the MS-T version of the MS method, it is not necessary to assign each torsional motion to a specific normal mode. The MS-T approximation reduces to the MS-LH approximation in the low-temperature limit, and it approaches the free-rotor result in the high-temperature limit. The Z_j and $f_{j,\tau}$ factors are designed to interpolate the partition functions between these limits in the intermediate temperature range. In principle, more accurate interpolations could be carried out[14] if one calculated the barrier heights for torsional motions that interconvert the reactant structures with one another and the transition state structures with one another, but an advantage of the method employed here is that it does not require this expensive step.

We define a single-structure (SS) rotational−vibrational partition function for structure j using the harmonic-oscillator approximation and including torsional anharmonicity, respectively

$$Q^{\text{SS-HO}}_{\text{rovib},j} = Q_{\text{rot},j} \exp(-U_j\beta) Q^{\text{HO}}_{\text{vib},j} \quad (3)$$

and

$$Q^{\text{SS-T}}_{\text{rovib},j} = Q_{\text{rot},j} \exp(-U_j\beta) Q^{\text{HO}}_{\text{vib},j} Z_j \prod_{\tau=1}^{t} f_{j,\tau} \quad (4)$$

Equation 3 is used to calculate the SS-HO partition functions for the single-structural variational theory (SS-VTST) calculations discussed in section 2.3. In the calculations of the present article, the structure retained is the one with the lowest energy, that is, $j = 1$.

We define $F^{Y}_{MS\text{-}X}$ as the ratio of the partition function calculated by the MS-T method to that calculated by SS-HO,

$$F^{Y}_{MS\text{-}X} = Q^{MS-X,Y}_{con-rovib}/Q^{SS\text{-}HO,Y}_{rovib,1} \quad (5)$$

where X = LH or T; Y = R, P, or ‡ (we use TS and ‡ interchangeably to denote the transition state). We call $F^{Y}_{MS\text{-}T}$ the multistructural torsional anharmonicity factor, whereas $F^{Y}_{MS\text{-}LH}$ is an intermediate result that includes all the structures, but not torsional anharmonicity. For brevity, $F^{Y}_{MS\text{-}LH}$ will be called the multiple-structure factor. Both $F^{Y}_{MS\text{-}T}$ and $F^{Y}_{MS\text{-}LH}$ are used in this paper for MP-VTST thermal rate constant calculations, with $F^{Y}_{MS\text{-}T}$ leading to our most reliable results and $F^{Y}_{MS\text{-}LH}$ being used to illustrate what would be predicted an intermediate level of statistical mechanical theory. Further details are discussed in section 2.4.

2.3. Multipath Variational Transition State Theory (MP-VTST) Rate Constants. For a unimolecular reaction, multipath variational transition state theory (MP-VTST) rate constants are calculated by

$$k^{MP\text{-}VTST} = \langle\gamma\rangle^{MP}_{p}\frac{1}{\beta h}\frac{Q^{\ddagger}_{el}Q^{MS-T,\ddagger}_{con-rovib}}{Q^{R}_{el}Q^{MS-T,R}_{con-rovib}}\exp(-\beta V^{\ddagger}) \quad (6)$$

where $\langle\gamma\rangle^{MP}_{P}$ is a path-averaged generalized transmission coefficient, P is the number of paths considered, β is $(k_B T)^{-1}$, k_B is Boltzmann's constant, h is Planck's constant, Q^{X}_{el} is electronic partition function for species X (X = R or TS), $V^{\ddagger}$ is a zero-point-exclusive barrier height (sometimes also called classical barrier height) which is the energy difference between the lowest-energy reactant structure and the lowest-energy saddle point. The energy of the lowest-energy reactant structure is set as the zero of energy in eq 6, and the zero of energy for the transition state partition function is the lowest-energy saddle point. The path-averaged generalized transmission coefficient $\langle\gamma\rangle^{MP}_{P}$ is discussed in section 2.4. To make the calculations more practical and the physical meaning of the formulism more clear as compared with the well-established variational transition state theory that uses only a single structure of the reactant and the saddle point, we rearrange eq 6 as

$$k^{MP\text{-}VTST} = \langle\gamma\rangle^{MP}_{p}F^{MS\text{-}X}(T)\frac{1}{\beta h}\frac{Q^{\ddagger}_{el}(T)Q^{SS\text{-}HO,\ddagger}_{rovib,k*}(T)}{Q^{R}_{el}(T)Q^{SS\text{-}HO}_{rovib,1}(T)}\exp(-\beta V^{\ddagger}_{k*}) \quad (7)$$

where k^* is a selected transition-state structure that can be any of the K saddle points; $V^{\ddagger}_{k^*}$ is the energy of structure k^* relative to the global minimum reactant structure; we use the global minimum of the reactant ($j = 1$ structure) for $Q^{SS\text{-}HO}_{rovib,1}(T)$ and $F^{MS\text{-}X}(T)$ is defined by

$$F^{MS\text{-}X} = \frac{F^{\ddagger}_{MS\text{-}X}(T)}{F^{R}_{MS\text{-}X}(T)} \quad (8)$$

where X = LH or T and the quantities on the right side of eq 8 were defined in eq 5. In greater detail, we have

$$F^{\ddagger}_{MS\text{-}X} = \frac{Q^{MS-X,\ddagger}_{con-rovib}(T)}{Q^{SS\text{-}HO,\ddagger}_{rovib,k*}(T)} \quad (9)$$

$$F^{R}_{MS\text{-}X} = \frac{Q^{MS-X,R}_{con-rovib}(T)}{Q^{SS\text{-}HO,R}_{rovib,1}(T)} \quad (10)$$

where $Q^{MS-X,\ddagger}_{con-rovib}(T)$ is the conformational−rotational−vibrational partition functions calculated using eqs 1 and 2.

If we set the generalized transmission coefficient $\langle\gamma\rangle^{MP}_{P}$ to unity, eq 7 reduces to the multistructural conventional transition state theory (MS-TST) rate

$$k^{MS\text{-}TST} = F^{MS\text{-}X}(T)\frac{1}{\beta h}\frac{Q^{\ddagger}_{el}(T)Q^{SS\text{-}HO,\ddagger}_{rovib,k*}(T)}{Q^{R}_{el}(T)Q^{SS\text{-}HO}_{rovib,1}(T)}\exp(-\beta V^{\ddagger}_{k*}) \quad (11)$$

For the two versions of the MS method (X = LH or T), the corresponding rate constants are labeled $k^{MS\text{-}TST}_{MS\text{-}LH}$ and $k^{MS\text{-}TST}_{MS\text{-}T}$, where the latter one includes not only multiple-structure anharmonicity, but also the torsional anharmonicity effect; thus, it is used in the final calculation of the MP-VTST rate constant.

If the multistructural anharmonicity factor $F^{MS\text{-}X}$ is set to unity, eq 10 is further reduced to the single-structure conventional transition state theory rate constant using the harmonic-oscillator approximation

$$k^{TST}_{SS\text{-}HO,k*}(T) = \frac{1}{\beta h}\frac{Q^{\ddagger}_{el}(T)Q^{SS\text{-}HO,\ddagger}_{rovib,k*}(T)}{Q^{R}_{el}(T)Q^{SS\text{-}HO}_{rovib,1}(T)}\exp(-\beta V^{\ddagger}_{k*}) \quad (12)$$

2.4. Path-Averaged Generalized Transmission Coefficients. In multipath variational transition state theory, the reactant, product, and transition state all have a multistructural anharmonicity with usually a different number of structures; but the number of reaction paths is equal to the number of transition state structures, and we denote this number as K as stated before. We label the structures of the transition state as k ($k = 1, 2, ..., K$), those of reactant as j ($j = 1, 2, 3, ..., J$), and those of product as l ($l = 1, 2, 3, ..., L$). The potential energy along each path, relative to the overall zero of energy, which is the potential energy of the lowest energy equilibrium structure of the reactants, is denoted as V_{MEP}. Each k labels a path, and the structures j and l that are connected with it by an MEP were used for MCSI calculations.

In practice, although the number of reaction paths is K, one can base the calcuations on a smaller number P, where $2 \le P \le K$. (When $P = 1$, the theory reduces to MS-VTST.) The calculated dynamic recrossing coefficient and transmission coefficient for path k are labeled as $\Gamma_k(T)$ and $\kappa_k(T)$. The path-averaged transmission coefficients and dynamical recrossing coefficients can be calculated using[36]

$$\langle\gamma\rangle^{MP}_{P} = \langle\Gamma(T)\kappa(T)g(T)\rangle_{P} = \frac{\sum_{k=1}^{P}\Gamma_k(T)\kappa_k(T)g_k(T)Q^{SS\text{-}HO,\ddagger}_{rovib,k}}{\sum_{k=1}^{P}Q^{SS\text{-}HO,\ddagger}_{rovib,k}} \quad (13)$$

where P is the number of paths considered, $\Gamma_k(T)$, $\kappa_k(T)$, and $g_k(T)$ are, respectively, the dynamic recrossing coefficient, transmission coefficient, and nonequilibrium coefficient of path k. We assume that $g_k(T)$ is equal to unity in the present work.

In a full treatment, eq 13 should include all the reaction paths, that is, P should be K. However, some paths have very large barrier heights, and their contribution to the path-averaged generalized transmission coefficient may be negligible at some temperatures because the weighting factor $Q^{SS\text{-}HO,\ddagger}_{rovib,k}$ is small due

Table 1. Calculated Forward and Reverse Zero-Point-Exclusive Barrier Heights and Energies of Reaction for the 1, 4-Hydrogen Shift Isomerization of 2-Cyclohexylethyl Radical[a]

method[b]	$V_f^{\ddagger}$	$V_r^{\ddagger}$	ΔE
CCSD(T)-F12a/jul-cc-pVTZ//M	25.63	27.75	−2.12
BMC−CCSD//M	25.66	27.51	−1.85
MCG3-TS//M	25.66	27.50	−1.84
M06-2X/MG3S	27.07	29.28	−2.21
M06-2X/aug-cc-pVTZ	27.14	29.36	−2.23
M06-2X/maug-cc-pVTZ	27.14	29.33	−2.19
M06-2X/def2-TZVP	27.04	29.20	−2.16
M08-SO/MG3S	26.73	29.16	−2.43
M08-SO/aug-cc-pVTZ	26.87	29.42	−2.55
M08-SO/maug-cc-pVTZ	26.79	29.29	−2.51
M08-SO/def2-TZVP	26.74	29.16	−2.42
M06/6-31+G(d,p)	26.09	28.61	−2.52

[a] As calculated by various methods (in kcal/mol). [b] //M is shorthand for //M06-2X/MG3S.

to high energy. Therefore, only those paths with the lowest barrier heights (more rigorously, with the largest $Q_{\mathrm{rovib},k}^{\mathrm{SS\text{-}HO},\ddagger}$) need to be considered in the calculation. Furthermore, it may not be necessary to include all paths that have a significant weight because we expect many low-energy paths have similar $\Gamma_k(T)$ and $\kappa_k(T)$. For example, if $\Gamma_k(T)\kappa_k(T)$ were the same for all paths, then $\langle\gamma\rangle_P^{\mathrm{MP}}$ would already reach its limiting value with $P = 1$, which was used previously.[8] In the present work, we choose to average over two reaction paths corresponding to TS structures $k = 1$ and $k = 2$, that is, $P = 2$.

For each reaction path, corresponding to a particular transition-state conformer (k), the MCSI method was utilized to obtain the MEP and ground-state vibrationally adiabatic potential curve (V_a^G), which were used to calculate the dynamical recrossing coefficients $\Gamma_k(T)$ and the transmission coefficient $\kappa_k(T)$ that incorporates the tunneling contributions using the small-curvature tunneling approximation[13,15] (SCT). The effective potential for tunneling is given by

$$V_a^G = V_{MEP}(s) + \varepsilon^G(s) \quad (14)$$

where s is the signed arc length along the MEP, $V_{MEP}(s)$ is the potential energy along the MEP, and $\varepsilon^G(s)$ is the local zero point energy (summed over all bound local vibrational modes). Note that the quantities in eq 14 should all have a label k, but we suppress the k dependence to keep the notation simpler. The MCSI[34] and MC-TINKERATE[35] programs were employed to carry out these calculations.

2.5. MCSI Algorithm for Potential Energy Surfaces. In the MCSI calculation for each path, the zero of energy for the potential energy surface is defined at the global minimum of the reactant, and we call that structure $j = 1$, and its potential energy is $U_1 = 0$ by definition. For each path, nine electronic-structure Shepard points (three stationary and six nonstationary) were used to build the potential energy surface by the MCSI method. All the information needed at Shepard points, namely, energies, gradients, and Hessians, was obtained by M06/6-31+G(d,p) calculations. The three stationary Shepard points were placed at the saddle point, reactant well, and product well for that path. The other six Shepard points are nonstationary points and were placed close to the minimum energy reaction path (MEP) using the strategy developed previously.[37]

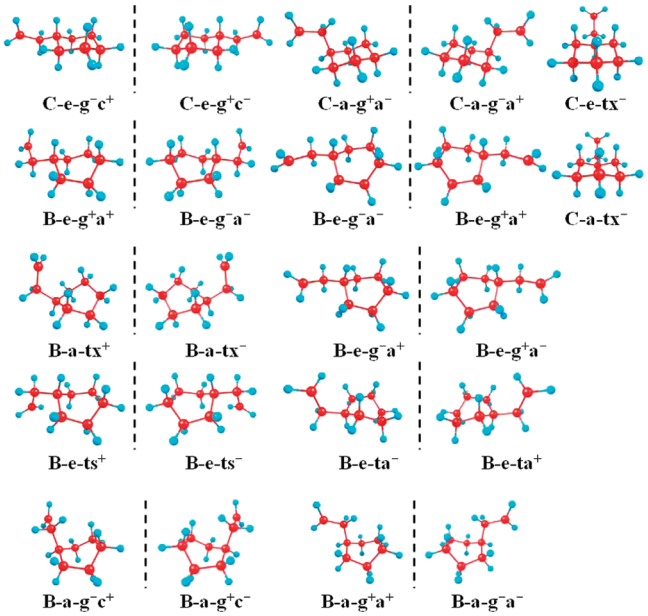

Figure 1. Structures (total of 22) of 2-cyclohexylethyl radical. Note that another name for this species is 2-cyclohexylethan-1-yl radical.

The MCSI method involves interpolating the off-diagonal element of a diabatic potential matrix[38−40] where the diagonal elements are given by molecular mechanics. We use the MM3 method[41−43] for the molecular mechanics. It was found that using a Morse potential for the C−H bond in the MM3 force field for the Shepard interpolation provided smoother V_a^G curves than using quadratic stretch potentials, and so we used Morse stretches for C−H bonds in all MM3 calculations. The Morse parameters are as follows: bond energy, 98 kcal/mol;[44] bond length, 1.12 Å;[39−41] and force constant, 4.74 N/cm.[40−42]

As discussed in previous work,[10] we used three different internal coordinate sets for MCSI calculations: set q for molecular mechanics calculations, set r for Shepard interpolation, and set s to calculate the Shepard weighting function. In the present work, set q is the standard set of MM3 internal coordinates, set r consists of 63 nonredundant internal coordinates (23 bond distances, 38 bond angles, and 2 dihedral angles), and set s consists of the three intra-atomic distances involving the atoms of the breaking and forming bonds.

Note that, in principle, the MCSI method provides the PES in a broad swath around a reaction path; where a region broad enough to calculate even the large-curvature tunneling effect, including multidimensional corning-cutting tunneling, is called a reaction swath.[45,46]

2.6. Arrhenius Activation Energies and Fitting of the Calculated Rate Constants. We calculate Arrhenius activation energies as

$$E_a = -R\frac{d\ln k}{d(1/T)} \quad (15)$$

for both the forward and reverse reactions, where R is the gas constant. We fit the calculated rate constants to the recently proposed[47] form given by

$$k = A\left(\frac{T}{300}\right)^n \exp\left[-\frac{E(T + T_0)}{R(T^2 + T_0^2)}\right] \quad (16)$$

dx.doi.org/10.1021/jp209146b | J. Phys. Chem. A 2012, 116, 297–308

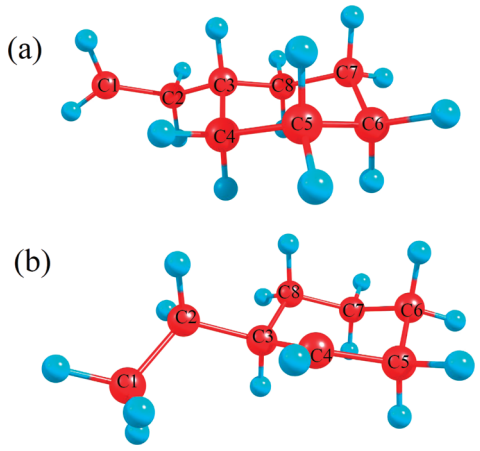

Figure 2. Numbering scheme for reactant (a) and product (b).

Table 2. Labeling of Structures[a]

C	chair
B	twisted boat
e	equatorial
a	axial

	abbreviation	dihedral angle range (deg)
antiperiplanar	$\mathbf{a}^+$	[140, 163]
	$\mathbf{a}^-$	[-163, −140]
gauche	$\mathbf{g}^+$	[55, 80]
	$\mathbf{g}^-$	[−80, −55]
syn	$\mathbf{x}^+$	[80, 130]
	$\mathbf{x}^-$	[−130, −80]
synclinal	$\mathbf{c}^+$	[30, 50]
	$\mathbf{c}^-$	[−50, −30]
trans	**t**	[−173, −180] and [180, 173]

[a] The dihedral angles used for torsions are and $H-C^{(3)}-C^{(2)}-C^{(1)}$ and $C^{(3)}-C^{(2)}-C^{(1)}-H$ for 2-cyclohexylethyl; the dihedral angle used for torsion is $H-C^{(3)}-C^{(2)}-C^{(1)}$ for *R*-2-ethylcyclohexan-1-yl.

which contains four parameters, A, n, T_0, and E. Based on eq 16, the Arrhenius activation energy E_a can be obtained by

$$E_a = E\frac{T^4 + 2T_0T^3 - T_0^2T^2}{(T^2 + T_0^2)^2} + nRT \qquad (17)$$

3. RESULTS AND DISCUSSION

3.1. Structures, Energetics, and Conformational−Vibrational−Rotational Partition Functions of Reactant, Product, and Saddle Point. Table 1 gives the zero-point-exclusive barrier heights and energies of reaction for the 1,4-hydrogen shift isomerization reaction of 2-cyclohexylethyl radical calculated by various theoretical methods. The CCSD(T)-F12a/may-cc-pVTZ//M calculation (where we use //M as shorthand for //M06−2X/MG3S) provides our best estimate. Barriers calculated by the BMC−CCSD//M and MCG3-TS//M multi-coefficient methods agree extremely well with each other (especially when one consider that these methods have quite different components) and with the best estimate. However, the M06-2X and M08-SO density functionals with the 6-31+G(d,p),

Table 3. Sequence Number and Energy[a] **(kcal/mol) of Structures of 2-Cyclohexylethyl Radical, *R*-2-Ethylcyclohexan-1-yl Radical, and the Transition State**

		energy	
structures	number	V	$V + \varepsilon^G$
	2-Cyclohexylethyl Radical		
C-e-g$^-$c$^+$, C-e-g$^+$c$^-$	$j = 1, j = 2$	0	129.46
C-a-g$^+$a$^+$, C-a-g$^-$a$^-$	$j = 3, j = 4$	1.42	133.06
C-e-tx$^-$	$j = 5$	0.50	130.66
C-a-tx$^-$	$j = 6$	3.86	137.57
B-e-g$^-$a$^+$, B-e-g$^+$a$^-$	$j = 7, j = 8$	6.06	141.60
B-e-g$^-$a$^-$, B-e-g$^+$a$^+$	$j = 9, j = 10$	6.14	141.76
B-a-tx$^+$, B-a-tx$^+$	$j = 11, j = 12$	6.48	142.71
B-e-g$^-$a$^+$, B-e-g$^+$a$^-$	$j = 13, j = 14$	6.55	142.62
B-e-ts$^+$, B-e-ts$^-$	$j = 15, j = 16$	6.63	142.88
B-e-ta$^-$, B-e-ta$^+$	$j = 17, j = 18$	6.82	143.17
B-a-g$^-$c$^+$, B-a-g$^+$c$^-$	$j = 19, j = 20$	7.09	143.94
B-a-g$^+$a$^+$, B-a-g$^-$a$^-$	$j = 21, j = 22$	7.43	144.59
	R-2-Ethylcyclohexan-1-yl		
C-e-g$^+$	$l = 1$	−2.21	127.44
C-e-g$^-$	$l = 2$	−2.14	127.82
C-e-t	$l = 3$	−1.94	128.56
C-a-g$^+$	$l = 4$	−1.21	130.81
C-a-g$^-$	$l = 5$	−0.69	132.49
C-a-t	$l = 6$	0.72	136.78
B-a-g$^+$	$l = 7$	2.37	141.41
B-a-g$^-$	$l = 8$	2.48	141.73
B-a-t	$l = 9$	4.14	146.82
	Transition State		
TS-1	$k = 1$	27.07	154.70
TS-2	$k = 2$	27.34	155.33
TS-3	$k = 3$	31.52	167.92
TS-4	$k = 4$	32.74	171.57

[a] V is the M06-2X/MG3S zero-point-exclusive energy of the structures, and $V + \varepsilon^G$ is the zero-point-inclusive energy that is calculated by adding the zero-point energy, which is calculated using M06-2X frequencies multiplied by a scale factor from ref 33. All energies in this table are relative to the classical equilibrium geometry of the $j = 1$ structure of the reactant.

MG3S, maug-cc-pVTZ, aug-cc-pVTZ, and def2-TZVP basis sets predict larger barrier heights. It is found that the M06 functional with the 6-31+G(d,p) basis gives results reasonably close to the CCSD(T)-F12a/may-cc-pVTZ//M calculation. Therefore, we chose M06/6-31+G(d,p) for the single-structural components of the kinetics calculation, that is, to calculate $k_{SS\text{-}HO}^{CVT}$ and κ^{SCT}. However, we expect M06-2X/MG3S to be more accurate for conformational energy differences, so we calculated $F^{MS\text{-}X}$ based on M06-2X/MG3S results.

The M06-2X/MG3S calculations show that 2-cyclohexylethyl radical, which contains two torsions and a six-membered ring, has 22 distinguishable structures (Figure 1). We label the molecule, as shown in Figure 2. The combination of the $C^{(1)}-C^{(2)}$ torsion and the $C^{(2)}-C^{(3)}$ torsion with the pseudorotation of the six-membered ring can produce many different conformers. The internal rotations around the $C^{(1)}-C^{(2)}$ and $C^{(2)}-C^{(3)}$ bonds generate torsional conformers, and the pseudorotation of the

dx.doi.org/10.1021/jp209146b |*J. Phys. Chem. A* 2012, 116, 297–308

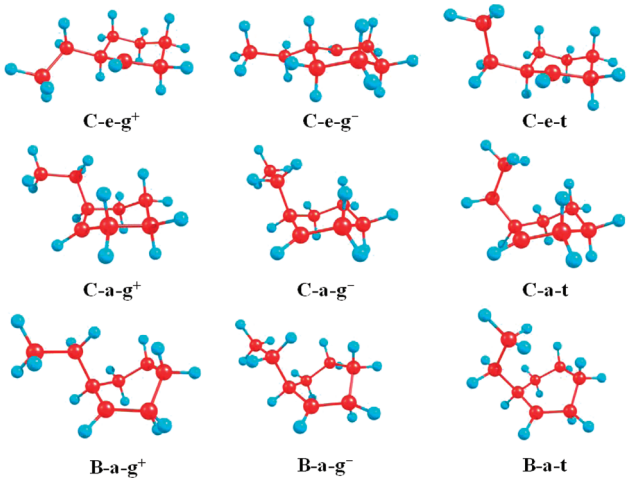

Figure 3. Nine structures of *R*-2-ethylcyclohexan-1-yl radical.

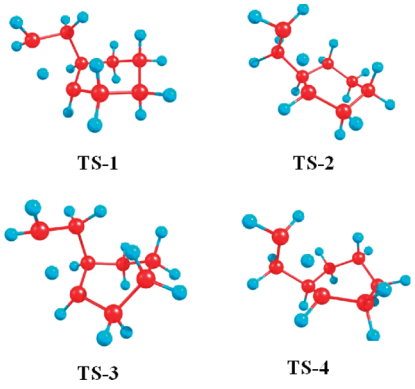

Figure 4. Four structures of transition state.

six-membered ring produces ring conformers, in particular, the chair equatorial (**C-e**), chair axial (**C-a**), twisted-boat equatorial (**B-e**), and twisted-boat axial (**B-a**) conformers. Table 2 and Figure 1 show the naming convention that is used for labeling of the structures. For example, **C-e-g$^-$g$^+$** means that the conformer of 2-cyclohexylethyl radical has a chair-equatorial ring structure and that the first and second exocyclic dihedral angles are in the ranges of −80 to −40 and 40 to 80 degrees, respectively. The numbering of the structures is specified in Table 3. It is found that structures 5 and 6 have a plane of symmetry, but the others do not, and they occur in mirror image pairs. The global minimum conformer is the mirror image pair **C-e-g$^-$g$^+$** and **C-e-g$^+$g$^-$**, and those structures with twisted-boat ring structure have an energy 6−7 kcal/mol higher than the global minimum.

The product, *R*-2-ethylcyclohexan-1-yl radical is labeled as Figure 2. The internal rotation around $C^{(1)}-C^{(2)}$ does not generate any distinguishable conformers. Therefore, only the torsion around $C^{(2)}-C^{(3)}$ bond and the pseudorotation of the ring produce conformers, and the resulting nine structures are displayed in Figure 3. None of these nine conformers forms a mirror image pair with any other.

Based on M06-2X calculations, the transition state between 2-cyclohexylethyl and *R*-2-ethylcyclohexan-1-yl radicals has four distinguishable structures (Figure 4). Unlike the reactant and product, the transition state structure has no internal rotation; instead, it contains two rigid rings. The energetic information of

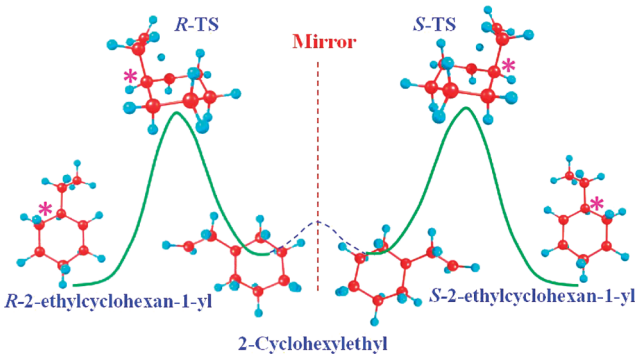

Figure 5. Mirror images of transition states and products in the reaction path.

Table 4. Calculated Conformational−Rotational−Vibrational Partition Function of 2-Cyclohexylethyl Radical Using Single-Structural and Multistructural Methods[a]

T (K)	SS-HO[b]	SS-T[c]	MS-LH	MS-T[d]
200	8.62×10^{-136}	1.02×10^{-135}	1.90×10^{-135}	2.24×10^{-135}
250	6.60×10^{-107}	7.89×10^{-107}	1.53×10^{-106}	1.82×10^{-106}
298.15	4.58×10^{-88}	5.50×10^{-88}	1.11×10^{-87}	1.33×10^{-87}
300	1.85×10^{-87}	2.22×10^{-87}	4.49×10^{-87}	5.38×10^{-87}
400	1.06×10^{-62}	1.26×10^{-62}	2.79×10^{-62}	3.31×10^{-62}
600	1.01×10^{-36}	1.16×10^{-36}	3.12×10^{-36}	3.52×10^{-36}
1000	3.72×10^{-13}	3.89×10^{-13}	1.64×10^{-12}	1.57×10^{-12}
1500	1.94×10^{2}	1.83×10^{2}	1.31×10^{3}	9.86×10^{2}
2000	4.01×10^{11}	3.40×10^{11}	3.68×10^{12}	2.24×10^{12}
2400	1.65×10^{17}	1.29×10^{17}	1.81×10^{18}	9.49×10^{17}

[a] All partition functions in this table have their zero of energy at the bottom of the potential well for the $j = 1$ structure of 2-cyclohexylethyl. [b] The partition function of the structure $j = 1$, **C-e-g$^-$c$^+$**, calculated using SS-HO approximation. [c] The partition function of the structure $j = 1$, **C-e-g$^-$c$^+$**, calculated using SS-T approximation. [d] The MS-T partition function is calculated using the MSTor program with NS/SC = 0:2.

the transition state structures is also given in Table 3, and we label these four structures **TS-1**, **TS-2**, **TS-3**, and **TS-4**, where **TS-1** and **TS-2** are the ones with lowest zero-point-inclusive energy at M06-2X/MG3S level. The structures of **C-a-g$^+$a$^+$** ($j = 3$) and **C-a-g$^+$** ($l = 4$) are the reactant and product structures that are connected with TS-1 by the MEP through TS-1; and the structures of **C-e-tx$^-$** ($j = 5$) and **C-e-t** ($l = 3$) are the reactant and product structures that are connected with TS-2 by the MEP through TS-2. As discussed in section 2.3, these are the structures that are used in the MCSI calculations.

Note that there is a second possible product, namely, *S*-2-ethylcyclohexan-1-yl radical, which is a mirror image of the *R* enantiomer. The transition states leading these two structures are also mirror images as illustrated in Figure 5. Therefore the rate constants are the same for these two reactions. Here we only report the rate constant for the reaction to produce *R*-2-ethylcyclohexan-1-yl radical.

We employed eqs 3 and 4 to calculate the partition functions of the structures **TS-1**, **C-e-g$^-$c$^+$**, and **C-e-g$^+$** using the SS-HO and SS-T approximations, respectively. The conformational-rovibrational partition functions of 2-cycloheylethyl, *R*-2-ethylcyclohexan-1-yl, and their transition state were evaluated by both

dx.doi.org/10.1021/jp209146b |*J. Phys. Chem. A* 2012, 116, 297–308

Table 5. Calculated Conformational−Rotational−Vibrational Partition Function of *R*-2-Ethylcyclohexan-1-yl Radical Using Single-Structural and Multistructural Methods[a]

T (K)	SS-HO[b]	SS-T[c]	MS-LH	MS-T[d]
200	6.92×10^{-136}	7.45×10^{-136}	1.16×10^{-135}	1.25×10^{-135}
250	6.05×10^{-107}	6.67×10^{-107}	1.08×10^{-106}	1.19×10^{-106}
298.15	4.58×10^{-88}	5.17×10^{-88}	8.65×10^{-88}	9.75×10^{-88}
300	1.86×10^{-87}	2.10×10^{-87}	3.52×10^{-87}	3.97×10^{-87}
400	1.19×10^{-62}	1.40×10^{-62}	2.44×10^{-62}	2.89×10^{-62}
600	1.26×10^{-36}	1.59×10^{-36}	2.92×10^{-36}	3.74×10^{-36}
1000	4.89×10^{-13}	6.50×10^{-13}	1.35×10^{-12}	1.83×10^{-12}
1500	2.61×10^{2}	3.36×10^{2}	8.38×10^{2}	1.10×10^{3}
2000	5.42×10^{11}	6.50×10^{11}	1.93×10^{12}	2.35×10^{12}
2400	2.23×10^{17}	2.51×10^{17}	8.46×10^{17}	9.61×10^{17}

[a] All partition functions in this table have their zero of energy at the bottom of the potential well for the $l = 1$ structure of *R*-2-ethylcyclohexan-1-yl. [b] The partition function of the structure $l = 1$, **C-e-g$^+$**, calculated using SS-HO approximation. [c] The partition function of the structure $l = 1$, **C-e-g$^+$**, calculated using SS-T approximation. [d] The MS-T partition function is calculated using the MSTor program with NS/SC = 2:0.

Table 6. Calculated Conformational−Rotational−Vibrational Partition Function of the Transition State Using Single-Structural and Multistructural Methods[a]

T (K)	SS-HO[b,c]	MS-LH[d]
200	2.70×10^{-134}	5.00×10^{-134}
250	6.31×10^{-106}	1.20×10^{-105}
298.15	1.94×10^{-87}	3.74×10^{-87}
300	7.63×10^{-87}	1.47×10^{-86}
400	1.41×10^{-62}	2.80×10^{-62}
600	3.90×10^{-37}	8.16×10^{-37}
1000	4.70×10^{-14}	1.13×10^{-13}
1500	1.29×10^{1}	3.69×10^{1}
2000	1.83×10^{10}	5.96×10^{10}
2400	6.03×10^{15}	2.14×10^{16}

[a] All partition functions in this table have their zero of energy at the bottom of the potential well for the $k = 1$ structure of the transition state. [b] The partition function of **TS-1**, calculated using the SS-HO approximation. [c] For the transition state, the partition function of **TS-1**, calculated using the SS-T approximation is the same as that by the SS-HO approximation and so it is not included in the table. [d] For the transition state the MS-T partition function is the same as that by the MS-LH approximation, and so only one of these approximations is shown.

of the MS-X methods[15,16] (that is, using both X = LH and X = T) using eqs 1 and 2, reviewed in section 2.2. The MS-T method should provide more accurate partition functions than either the single-structural or MS-LH approximations. All the calculated partition functions of the reactant, product, and transition state are given in Tables 4−6.

For 2-cyclohexylethyl, the torsions around the $C^{(1)}-C^{(2)}$ and $C^{(2)}-C^{(3)}$ bonds are strongly coupled[15] (SC), thus, we carried out the partition function calculations using the scheme[15] labeled NS:SC = 0:2, which denotes no nearly separable (NS) torsions and two strongly coupled ones. By contrast, *R*-2-ethylcyclohexan-1-yl has two nearly separable torsions; thus the partition calculation scheme for this case is NS:SC = 2:0. The transition state does not have any torsion; therefore, MS-T reduces to MS-LH automatically. All the information of each reactant, product, and transition-state structure used for the partition function calculations carried out by the MSTor program is given Tables 7 and 8.

Table 7. Information Used for 2-Cyclohexylethyl Radical Partition Function Using the MS-T Method[a]

torsion	$\bar{\omega}$	I	W	M
		Structures 1 and 2		
C(1)−C(2)	136.01	1.72	306.77	2.48
C(2)−C(3)	114.00	18.28	2291.71	2.48
		Structures 3 and 4		
C(1)−C(2)	144.55	1.72	349.05	2.47
C(2)−C(3)	100.02	20.23	1968.11	2.47
		Structure 5		
C(1)−C(2)	115.69	1.71	237.70	2.39
C(2)−C(3)	108.66	19.65	2410.02	2.39
		Structure 6		
C(1)−C(2)	190.47	1.71	631.82	2.41
C(2)−C(3)	88.82	19.76	1591.87	2.41
		Structures 7 and 8		
C(1)−C(2)	130.684	1.72	73.186	4.88
C(2)−C(3)	124.278	17.756	683.117	4.88
		Structures 9 and 10		
C(1)−C(2)	134.36	1.72	79.64	4.81
C(2)−C(3)	124.70	18.27	728.28	4.81
		Structures 11 and 12		
C(1)−C(2)	134.12	1.71	156.90	3.41
C(2)−C(3)	132.38	19.77	1767.06	3.41
		Structures 13 and 14		
C(1)−C(2)	106.47	1.72	88.60	3.61
C(2)−C(3)	122.80	18.15	1245.58	3.61
		Structures 15 and 16		
C(1)−C(2)	124.81	1.71	82.48	4.38
C(2)−C(3)	121.76	19.59	898.19	4.38
		Structures 17 and 18		
C(1)−C(2)	93.76	1.72	32.34	5.26
C(2)−C(3)	144.74	19.23	863.52	5.26
		Structures 19 and 20		
C(1)−C(2)	147.02	1.72	179.83	3.50
C(2)−C(3)	120.30	20.64	1446.64	3.50
		Structures 21 and 22		
C(1)−C(2)	142.06	1.72	168.89	3.49
C(2)−C(3)	119.84	19.55	1367.49	3.49

[a] We used NS/SC = 0:2 and M06-2X/MG3S for this table. The units are cm^{-1} for torsional barrier heights W and frequencies $\bar{\omega}$. The unit is amu Å^2 for internal moments of inertia, I; and the local periodicity M is unitless. See ref 11 for details of the method.

Table 4 shows that, at low temperature (200−250 K), the partition functions calculated by MS-LH and MS-T for 2-cyclohexylethyl are within 5−9%, and as the temperature increases,

dx.doi.org/10.1021/jp209146b |*J. Phys. Chem. A* 2012, 116, 297–308

Table 8. Information Used for *R*-2-Ethylcyclohexan-1-yl Radical Partition Function Using the MS-T Method[a]

torsion	$\bar{\omega}$	I	W	M
		Structure 1		
C(1)−C(2)	204.38	3.07	846.24	3
C(2)−C(3)	115.60	20.21	1780.14	3
		Structure 2		
C(1)−C(2)	227.97	3.07	1052.35	3
C(2)−C(3)	99.95	20.14	1326.05	3
		Structure 3		
C(1)−C(2)	212.94	3.10	925.10	3
C(2)−C(3)	105.96	20.75	1535.79	3
		Structure 4		
C(1)−C(2)	227.31	3.08	1048.25	3
C(2)−C(3)	90.31	22.53	1210.96	3
		Structure 5		
C(1)−C(2)	230.12	3.07	1071.97	3
C(2)−C(3)	87.30	22.38	1124.07	3
		Structure 6		
C(1)−C(2)	277.09	3.10	1567.09	3
C(2)−C(3)	115.27	21.56	1888.53	3
		Structure 7		
C(1)−C(2)	226.07	3.08	1038.02	3
C(2)−C(3)	98.84	21.92	1411.65	3
		Structure 8		
C(1)−C(2)	226.59	3.07	1039.77	3
C(2)−C(3)	99.92	22.83	1502.11	3
		Structure 9		
C(1)−C(2)	249.374	3.09	1268.04	3
C(2)−C(3)	106.41	21.78	1624.98	3

[a] We used NS/SC = 2:0 and M06-2X/MG3S for this table. The units are cm^{-1} for torsional barrier heights W and frequencies $\bar{\omega}$; the unit is amu $Å^2$ for internal moments of inertia, I; and the local periodicity M is unitless. See ref 11 for details of the method.

the MS-LH approximation changes from being an underestimate to being an overestimate by a factor of up to 1.9. Table 5 shows that the deviations are smaller for *R*-2-ethylcyclohexan-1-yl, where they are less than a factor of 1.4 over the entire temperature range. For the transition state, the MS-T and MS-LH partition functions are identical, and they are given in Table 6.

3.2. Path-Averaged Transmission Coefficients and Dynamic Recrossing Coefficients. Given that **TS-3** and **TS-4** have higher values of V_a^G than **TS-1** and **TS-2**, we average only over the reaction paths crossing **TS-1** (path 1) and **TS-2** (path 2) for the path-averaged transmission coefficients and dynamic recrossing coefficients calculation using eq 13. For path 1, the MCSI method uses the structure **TS-1** as the transition state and structures **C-a-g$^+$a$^+$** and **C-a-g$^+$** as the reactant and product wells; and for path 2, **TS-2** is the transition state, and **C-e-tx$^-$** and **C-e-t** locate in the reactant and product wells. For each path, three stationary and six nonstationary Shepard points are used to obtain well converged V_{MEP} and V_a^G curves. The calculated V_{MEP} and V_a^G curves are displayed in Figures 6 and 7 by plotting $V_{MEP} - V^{\ddagger}$ and $V_a^G - V_a^{AG}$, where V_a^{AG} is the maximum of a V_a^G curve.

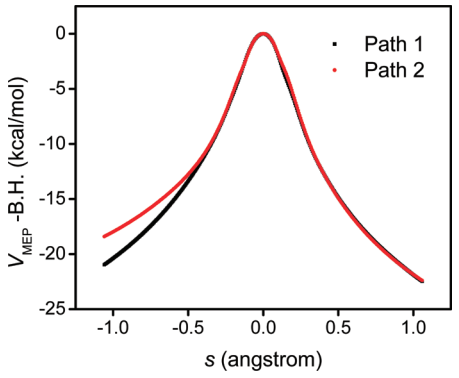

Figure 6. Calculated V_{MEP} vs the reaction coordinate s (scaled to a reduced mass of one amu) for the 1,4-hydrogen shift isomerization reaction of 2-cyclohexylethyl radical. This figure is based on M06/6-31+G(d,p). B.H. represents the barrier height.

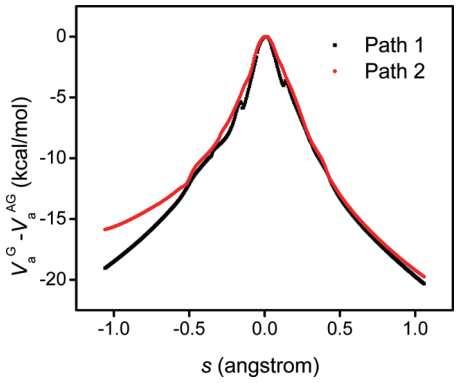

Figure 7. Calculated ground-state vibrationally adiabatic potential (V_a^G) vs the reaction coordinate s (scaled to a reduced mass of one amu) for the 1,4-hydrogen shift isomerization reaction of 2-cyclohexylethyl radical. This figure is based on M06/6-31+G(d,p).

The V_a^G curves are used to calculate transmission coefficients by the SCT approximation, and the results of path-averaged transmission coefficients and dynamical recrossing coefficients are listed in Table 9. Figure 6 shows that paths 1 and 2 have very similar V_{MEP} profiles in the range of s from −0.5 to 1.0 Å. But the potential energy profile along path 1 is a little thinner than that along path 2 in the range of 0.1−0.3 Å. From −0.5 to −1.0 Å, the V_{MEP} profile of path 2 is higher than that of path 1. The V_a^G curve of path 2 is smoother than that of path 2, and the V_a^G curve of path 1 is thinner than that of path 2. Although the nonsmoothness of path 1 complicates the comparison of the two V_a^G curves, the region close to the saddle point seems trustable, and already in this region, Figure 7 shows that path 1 is thinner than path 2. Consequently, κ_1 is around 12, 9, 5, and 2 times larger than κ_2 at 250, 300, 400, and 600 K, respectively. In addition, the dynamic recrossing coefficients Γ_1 and Γ_2 are close to each other. These calculations show that the reaction has a very large generalized transmission coefficient $\langle\gamma\rangle_2^{MP}$ below 500 K. In particular, it increases the TST rate constant by factors of 1.8, 6.2, 4350, and 2.15×10^5 at 1000, 600, 300, and 250 K, respectively. Above 1000 K, it increases the rate by less than 80%.

3.3. SS-TST and Rate Constants. We select **TS-1** for the single-structure TST rate constant calculation, as discussed in section 2.3; thus, $k^* = 1$ (**TS-1**) in the current study. The forward

dx.doi.org/10.1021/jp209146b |*J. Phys. Chem. A* 2012, 116, 297–308

Table 9. Dynamic Crossing and Transmission Coefficients Calculated Using Small-Curvature Tunneling Approximation at Various Temperatures Based on Reaction Paths 1 and 2 Calculated by MCSI and MC-TINKERATE

	$\Gamma_k(T)$		$\kappa_k(T)$		
T/K	path 1	path 2	path 1	path 2	$\langle\Gamma(T)\kappa(T)\rangle_2$
200	8.97×10^{-1}	9.60×10^{-1}	7.78×10^{8}	3.65×10^{7}	1.89×10^{8}
250	9.05×10^{-1}	9.69×10^{-1}	6.92×10^{5}	5.96×10^{4}	2.15×10^{5}
298.15	9.07×10^{-1}	9.73×10^{-1}	1.36×10^{4}	1.59×10^{3}	4.86×10^{3}
300	9.06×10^{-1}	9.74×10^{-1}	1.21×10^{4}	1.43×10^{3}	4.35×10^{3}
400	9.12×10^{-1}	9.84×10^{-1}	1.88×10^{2}	4.03×10^{1}	8.56×10^{1}
600	9.07×10^{-1}	9.84×10^{-1}	9.59	4.67	6.22
1000	9.05×10^{-1}	9.85×10^{-1}	2.23	1.72	1.84
1500	8.98×10^{-1}	9.84×10^{-1}	1.42	1.27	1.26
2000	8.99×10^{-1}	9.82×10^{-1}	1.21	1.15	1.11
2400	8.96×10^{-1}	9.82×10^{-1}	1.14	1.10	1.05

Table 10. Forward SS-TST and MP-VTST Thermal Rate Constants (in s^{-1}) for the 1,4-Hydrogen Shift Isomerization Reaction of 2-Cyclohexylethyl Radical To Produce *R*-2-Ethylcyclohexan-1-yl Radical at Various Temperatures[a]

T (K)	$k^{TST}_{SS\text{-}HO,1}$	$k^{TST}_{SS\text{-}T,1}$	$k^{MP\text{-}CVT/SCT}_{MS\text{-}LH}$	$k^{MP\text{-}CVT/SCT}_{MS\text{-}T}$
200	4.57×10^{-15}	3.91×10^{-15}	7.26×10^{-7}	6.21×10^{-7}
250	8.59×10^{-10}	7.24×10^{-10}	1.52×10^{-4}	1.28×10^{-4}
298.15	2.16×10^{-6}	1.82×10^{-6}	8.37×10^{-3}	7.08×10^{-3}
300	2.78×10^{-6}	2.34×10^{-6}	9.66×10^{-3}	8.12×10^{-3}
400	6.67×10^{-2}	5.68×10^{-2}	4.30	3.69
600	1.62×10^{3}	1.45×10^{3}	6.82×10^{3}	6.20×10^{3}
1000	5.60×10^{6}	5.54×10^{6}	5.57×10^{6}	6.09×10^{6}
1500	3.52×10^{8}	4.00×10^{8}	1.87×10^{8}	2.72×10^{8}
2000	2.86×10^{9}	3.70×10^{9}	1.13×10^{9}	2.10×10^{8}
2400	8.23×10^{9}	1.19×10^{10}	2.81×10^{9}	6.20×10^{9}

[a] Includes variational effects, torsional anharmonicity, and tunneling.

and reverse single-structural rate constants $k^{TST}_{SS\text{-}HO,1}$ and $k^{TST}_{SS\text{-}T,1}$ are calculated by the SS-HO and the SS-T approximations using eq 12. The reactant and product for SS calculations are structures $j = 1$ and $l = 1$, which are **C-e-g$^-$c$^+$** and **C-e-g$^+$**. Both of these two rate constants only include one structure in the reactant and transition state, but they treat the internal rotations differently. Note that the SS-HO and SS-T rate constants are based on the same transition state partition functions because there is no torsional motion in the transition state, but the reactant partition function has a different trend as a function of temperature in these two approximations. The SS-T approximation provides a more accurate result because it approaches the free rotor partition function at the high temperature limit. By contrast, SS-HO overestimates the partition function at high temperature. Therefore, the SS-HO approximation makes the rate constant smaller in the high-temperature range. The results are given in the first and second rate constant columns of Tables 10 and 11. The results, given in the SS columns of Table 10, show that the forward rate constant $k^{TST}_{SS\text{-}HO,1}$ is larger than $k^{TST}_{SS\text{-}T,1}$ below 1500 K, but the trend is opposite at higher temperature. Table 11 shows that the SS-HO and SS-T results agree much better for the reverse reaction with the largest deviation being a factor of 1.28 at 1000 K.

Table 11. SS-TST and MP-VTST Thermal Rate Constants (in s^{-1}) for the 1,4-Hydrogen Shift Isomerization Reaction of *R*-2-Ethylcyclohexan-1-yl Radical To Produce 2-Cyclohexylethyl Radical at Various Temperatures[a]

T (K)	$k^{TST}_{SS\text{-}HO,1}$	$k^{TST}_{SS\text{-}T,1}$	$k^{MP\text{-}CVT/SCT}_{MS\text{-}LH}$	$k^{MP\text{-}CVT/SCT}_{MS\text{-}T}$
200	7.02×10^{-17}	6.57×10^{-17}	1.46×10^{-8}	1.37×10^{-8}
250	2.66×10^{-11}	2.43×10^{-11}	6.09×10^{-6}	5.55×10^{-6}
298.15	1.05×10^{-7}	9.42×10^{-8}	5.21×10^{-4}	4.68×10^{-4}
300	1.37×10^{-7}	1.22×10^{-7}	6.10×10^{-4}	5.47×10^{-4}
400	5.88×10^{-3}	5.04×10^{-3}	4.88×10^{-1}	4.18×10^{-1}
600	2.57×10^{2}	2.08×10^{2}	1.44×10^{3}	1.16×10^{3}
1000	1.45×10^{6}	1.14×10^{6}	2.31×10^{6}	1.80×10^{6}
1500	1.18×10^{8}	9.77×10^{7}	1.32×10^{8}	1.10×10^{8}
2000	1.09×10^{9}	1.00×10^{9}	1.11×10^{9}	1.03×10^{9}
2400	3.36×10^{9}	3.36×10^{9}	3.31×10^{9}	3.38×10^{9}

[a] Includes variational effects, torsional anharmonicity, and tunneling. Note that the reaction in this table is the reverse of that in Table 10.

Table 12. Multiple-Structure Anharmonicity Factors $F_{MS\text{-}LH}$ and Multistructural Torsional Anharmonicity Factors $F_{MS\text{-}T}$ with Respect to the Structures TS-1 for the Transition State, C-e-g$^+$g$^-$ for the Reactant, and C-e-g$^+$ for the Product

	$F^{\ddagger}_{MS\text{-}X}$		$F^{R}_{MS\text{-}X}$		$F^{P}_{MS\text{-}X}$	
T (K)	HO	T	HO	T	HO	T
200	1.85	1.85	2.20	2.60	1.68	1.80
250	1.90	1.90	2.31	2.77	1.79	1.97
298.15	1.93	1.93	2.42	2.90	1.89	2.13
300	1.93	1.93	2.42	2.91	1.89	2.13
400	1.99	1.99	2.64	3.13	2.06	2.44
600	2.09	2.09	3.08	3.48	2.32	2.97
1000	2.40	2.40	4.41	4.22	2.76	3.73
1500	2.85	2.85	6.75	5.08	3.21	4.21
2000	3.26	3.26	9.17	5.58	3.56	4.34
2400	3.54	3.54	10.95	5.75	3.79	4.30

3.4. Multistructural Anharmonicity Factors. Table 12 gives $F^{\ddagger}_{MS\text{-}X}$, $F^{R}_{MS\text{-}X}$, and $F^{P}_{MS\text{-}X}$ (X = LH or T) for the transition state, reactant, and product at various temperatures. It shows that the multiple-structure factors $F^{Y}_{MS\text{-}LH}$ (Y = TS, R, or P) are in the range 1.9−3.5, 2.2−11, and 1.7−3.8, respectively, and the multistructural torsional anharmonicity factors $F^{Y}_{MS\text{-}T}$ are spread over the range 1.9−3.5, 2.6−5.8, and 1.8−4.3, respectively. Note that the transition state has no torsion so that $F^{\ddagger}_{MS\text{-}LH}$ and $F^{\ddagger}_{MS\text{-}T}$ are identical. To understand the trends in the multistructural torsional anharmonicity factor $F^{Y}_{MS\text{-}T}$, it is useful to factor it as

$$F^{Y}_{MS\text{-}T} = F^{Y}_{MS\text{-}LH} F^{Y}_{tor} \tag{18}$$

where $F^{Y}_{MS\text{-}LH}$ is defined in eq 5 and F^{Y}_{tor} is called the torsional factor, which is defined as

$$F^{Y}_{tor} = \frac{Q^{MS\text{-}T,\,Y}_{con\text{-}rovib}(T)}{Q^{MS\text{-}LH,\,Y}_{con\text{-}rovib}(T)} \tag{19}$$

Figures 8−10 show the two factors at various temperatures for the reactant, transition state, and product, respectively. It is found

dx.doi.org/10.1021/jp209146b | J. Phys. Chem. A 2012, 116, 297–308

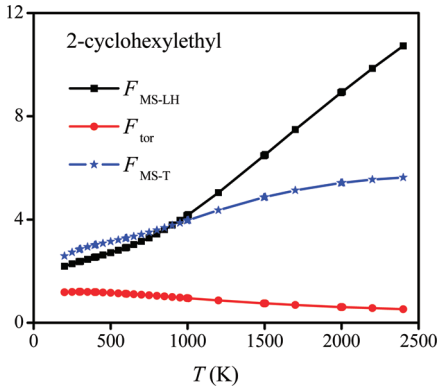

Figure 8. Multistructural anharmonicity factors (blue), multiple-structure factors (black), and torsional factors (red) of 2-cyclohexylethyl at various temperatures.

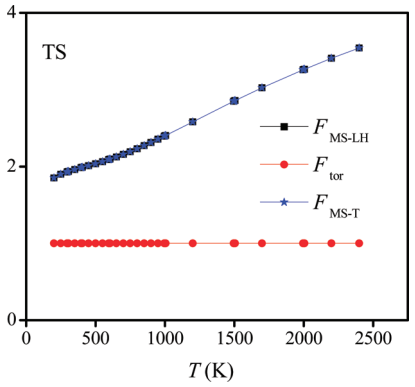

Figure 9. Multistructural anharmonicity factors (blue), multiple-structure factors (black), and torsional factors (red) of the transition state (TS) at various temperatures T. Note that multistructural anharmonicity factors (blue) and multiple-structure factors (black) are identical in this case.

that F^{Y}_{MS-LH} and F^{Y}_{tor} show different trends with increasing temperature. F^{Y}_{MS-LH} is a monotonically increasing function of temperature. As T increases, those structures with higher conformation energy make a greater contribution to the partition function $Q^{MS-LH,Y}_{con-rovib}(T)$. By contrast, F^{Y}_{tor} for 2-cyclohexylethyl decays with increasing temperature above 500 K; and F^{Y}_{tor} for *R*-2-ethylcyclohexan-1-yl first slightly increases with T in the temperature range 200−1000 K, and then it decrease above 1000 K. The transition state has no torsion; thus, its F^{Y}_{tor} is 1.0 over the whole temperature range.

The reactant has the largest number of conformers; and as a consequence it has the largest multiple-structure factors over the whole 200 to 2400 K temperature range. However, although the reactant has 22 conformers, F^{R}_{MS-LH} is only 2.2−2.6 in the low-temperature and slightly above room-temperature range of 200−400 K although it rises to 10.95 at 2400 K. The fact that the multiple-structure factors are much less than the number of structures over the whole temperature range for reactant may be attributed to the fact such that the twisted-boat conformers are high in energy relative to the global minimum structure. Nevertheless, their contribution to the total partition function increases with temperature, and they do play a significant role when temperature is high enough.

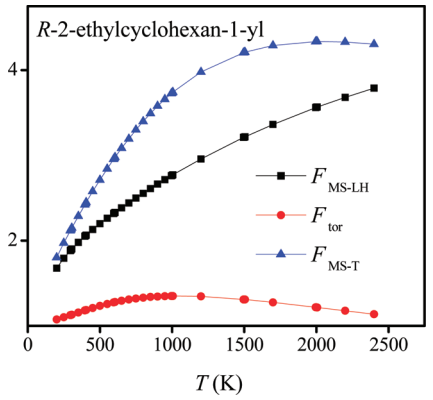

Figure 10. Multistructural anharmonicity factors (blue), multiple-structure factors (black), and torsional factors (red) of *R*-2-ethylcyclohexan-1-yl at various temperatures.

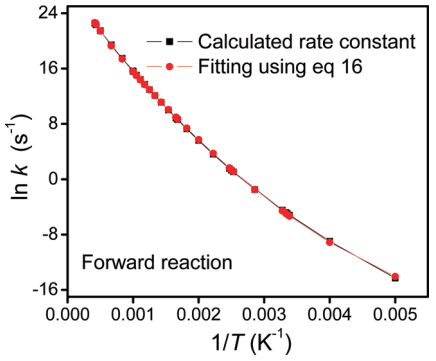

Figure 11. Arrhenius plots of calculated forward rate constant $k^{MP-CVT/SCT}_{MS-T}$, calculated by MP-VTST (black curve).

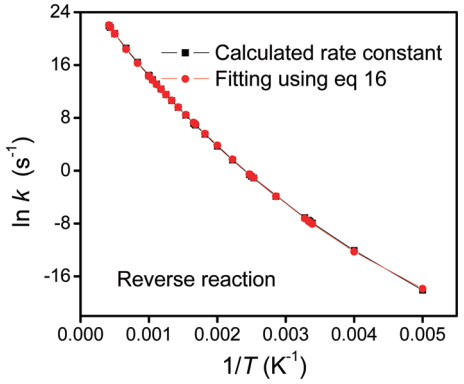

Figure 12. Arrhenius plots of calculated reverse rate constant $k^{MP-CVT/SCT}_{MS-T}$, calculated by MP-VTST (black curve).

3.5. Final Thermal Rate Constants and Arrhenius Activation Energy. We calculate the final MP-VTST/SCT thermal rate constant using eq 6. The results are given in the MP columns of Tables 10 and 11; Figures 11 and 12 display the calculated forward and reverse rate constants over the temperature range of 200−2400 K.

We note that the forward $k^{MP-CVT/SCT}_{MS-T}$ is lower than $k^{MP-CVT/SCT}_{MS-LH}$ by factors of 0.85 and 0.91at 200 and 600 K. But at 2400 K, $k^{MP-CVT/SCT}_{MS-T}$ is larger than $k^{MP-CVT/SCT}_{MS-LH}$ by a factor of 2.2.

dx.doi.org/10.1021/jp209146b |*J. Phys. Chem. A* 2012, 116, 297–308

Table 13. Forward and Reverse Activation Energy (in kcal/mol), Calculated by MP-VTST for the 1,4-Hydrogen Shift Isomerization Reaction of 2-Cyclohexylethyl Radical at Various Temperatures and for the Reverse Reaction

T (K)	300	400	600	1000	1500	2000	2300	2400
forward (MP-CVT/SCT)[a]	13.2/13.6	15.5/16.5	19.2/19.0	21.9/21.4	23.4/24.0	24.0/26.8	26.1/28.6	26.3/29.2
reverse (MP-CVT/SCT)[a]	14.4/14.9	16.9/17.7	20.4/20.2	23.6/22.9	26.2/26.2	26.4/29.6	28.2/31.8	28.4/32.5

[a] The first number is calculated using eq 15, and the second one is calculated using eq 17, based on the fitting results.

Table 13 shows the Arrhenius activation energy E_a, calculated by eq 15, based on $k_{MS\text{-}T}^{MP\text{-}CVT/SCT}$. Table 13 shows that E_a increases with temperature but much more slowly than linearly in T, in disagreement with the linearity predicted by the usual fitting expression, which is consistent with our previous[47] finding. Thus, we employ eq 16 to fit the rate constant for both forward and reverse reactions, and the fitting plots are displayed in Figures 11 and 12. We obtain the following fitting parameters: $A = 1.00 \times 10^8$ s^{-1}, $n = 3.30$, $E = 11.87$ kcal/mol, and $T_0 = 182.83$ K for the forward reaction; $A = 1.55 \times 10^7$ s^{-1}, $n = 3.94$, $E = 12.18$ kcal/mol, and $T_0 = 171.11$ K for the reverse reaction. The results are also listed in Table 13. It shows that the Arrhenius activation energy E_a predicted using eq 15 agree very well with that calculated using eq 17 in the temperature range 300−1500 K for both forward and reverse reactions. At 2000−2400 K, the deviation gets large.

4. CONCLUSION

We proposed a new formulation of VTST called MP-VTST. It is based on the recent MS-VTST formulation, but it extends that formulation to incorporate multiple paths in the calculation of the tunneling transmission coefficient and the variational effect. To demonstrate MP-VTST, we apply it to calculate both the forward and reverse reaction rate constant of the 1,4-hydrogen shift reaction of 2-cyclohexylethyl radical in the temperature range from 200 to 2400 K. This reaction has 23 atoms (C_8H_{15}), and a major challenge in predicting the thermal rate constant in the current study is that the reactant, product, and transition state each have many structures that make the potential energy surface and partition functions used in the rate calculations very complex. We average over two reaction paths, and we use multiconfiguration Shepard interpolation (MCSI) to obtain a semiglobal potential energy surface that is used to calculate V_{MEP} and V_a^G potential energy curves for each of the reaction paths. The MCSI method uses molecular mechanics to facilitate an efficient interpolation of density functional calculations. MCSI provides, with only nine electronic structure Hessians, a good enough interpolation of the 63-dimensional potential energy surface to calculate path-averaged generalized transmission coefficients using the SCT approximation. Then the multistructural anharmonicity factors, which include both multiple-structure and torsional anharmonicity effects, were evaluated using the MS-T approximation by using the MSTor program. Finally, the thermal rate constants were calculated as the product of the SS-VTST rate constant with the harmonic approximation (calculated by using the POLYRATE program[48]), the path-averaged generalized transmission coefficient, and the multistructural anharmonicity factor.

AUTHOR INFORMATION

Corresponding Author

*E-mail: truhlar@umn.edu.

ACKNOWLEDGMENT

The authors are grateful to Wing Tsang for emphasizing the importance of this reaction as a prototype for thermochemical kinetics. This work was supported by the U.S. Department of Energy, Office of Basic Energy Sciences under Grant No. DE-FG02-86ER13579 and by the Combustion Energy Frontier Research Center under Award No. DE-SC0001198.

REFERENCES

(1) Miyoshi, A.; Widjaja, J.; Yamauchi, N.; Koshi, M.; Matsui, H. *Proc. Combust. Inst.* **2002**, *29*, 1285.
(2) Yamauchi, N.; Miyoshi, A.; Kosaka, K.; Koshi, M.; Matsui, H. *J. Phys. Chem. A* **1999**, *103*, 2723.
(3) Tsang, W.; Walker, J. A.; Manion, J. A. *Proc. Combust. Inst.* **2007**, *31*, 141.
(4) Zheng, J.; Truhlar, D. G. *J. Phys. Chem. A* **2009**, *113*, 11919.
(5) Truhlar, D. G.; Kuppermann, A. *J. Am. Chem. Soc.* **1971**, *93*, 1840.
(6) Baldridge, K. K.; Gordon, M. S.; Steckler, R.; Truhlar, D. G. *J. Phys. Chem.* **1989**, *93*, 5107.
(7) Truhlar, D. G. In *The Reaction Path in Chemistry: Current Approaches and Perspectives*; Heidrich, D., Ed.; Kluwer: Dordrecht, 1995; p 229.
(8) Yu, T. T.; Zheng, J.; Truhlar, D. G. *Chem. Sci.* **2011**, *2*, 2199.
(9) Kim, Y.; Corchado, J. C.; Villa, J.; Xing, J.; Truhlar, D. G. *J. Chem. Phys.* **2000**, *112*, 2718.
(10) Tishchenko, O.; Truhlar, D. G. *J. Phys. Chem. A* **2006**, *110*, 13530.
(11) Zheng, J.; Yu, T.; Papajak, E.; Alecu, I. M.; Mielke, S. L.; Truhlar, D. G. *Phys. Chem. Chem. Phys.* **2011**, *13*, 10885.
(12) Truhlar, D. G.; Isaacson, A. D.; Skodje, R. T.; Garrett, B. C. *J. Phys. Chem.* **1982**, *86*, 2252.
(13) Fernandez-Ramos, A.; Ellingson, B. A.; Garrett, B. C.; Truhlar, D. G. *Rev. Comput. Chem.* **2007**, *23*, 125.
(14) (a) Zhao, Y.; Truhlar, D. G. *Theor. Chem. Acc.* **2008**, *120*, 215. (b) Zhao, Y.; Truhlar, D. G. *Theor. Chem. Acc.* **2008**, *119*, 525.
(15) Liu, Y.-P.; Lynch, G. C; Truong, T. N.; Lu, D.-h.; Truhlar, D. G.; Garrett, B. C. *J. Am. Chem. Soc.* **1993**, *115*, 2408.
(16) Zheng, J,; Mielke, S. L.; Clarkson, K. L.; Truhlar, D. G. *MSTor*, computer program, version 2011; University of Minnesota: Minneapolis, 2011.
(17) (a) Krishnan, R.; Binkley, J. S.; Seeger, R.; Pople, J. A. *J. Chem. Phys.* **1980**, *72*, 650. (b) Clark, T.; Chandrasekhar, J.; Spitznagel, G. W.; Schleyer, P. v. R. *J. Comput. Chem.* **1983**, *4*, 294. (c) Frisch, M. J.; Pople, J. A.; Binkley, J. S. *J. Chem. Phys.* **1984**, *80*, 3265.
(18) Lynch, B. J.; Zhao, Y.; Truhlar, D. G. *J. Phys. Chem. A* **2003**, *107*, 1384.
(19) Zhao, Y.; Truhlar, D. G. *J. Chem. Theor. Comput.* **2008**, *4*, 1849.
(20) Lynch, B. J.; Zhao, Y.; Truhlar, D. G. *J. Phys. Chem. A* **2005**, *109*, 1643.
(21) Zhao, Y.; Lynch, B. J.; Truhlar, D. G. *Phys. Chem. Chem. Phys.* **2005**, *7*, 43.
(22) Adler, T. B.; Knizia, G.; Werner, H.-J. *J. Chem. Phys.* **2007**, *127*, 221106.
(23) Knizia, G; Adler, T. B.; Werner, H.-J. *J. Chem. Phys.* **2009**, *130*, 054104.
(24) Clark, T.; Chandrasekhar, J.; Spitznagel, G. W.; Schleyer, P. v. R. *J. Comput. Chem.* **1983**, *4*, 294.
(25) Papajak, E.; Leverentz, H. R.; Zheng, J.; Truhlar, D. G. *J. Chem. Theor. Comput.* **2009**, *5*, 1197.
(26) (a) Dunning, T. H., Jr. *J. Chem. Phys.* **1989**, *90*, 1007. (b) Kendall, R. A.; Dunning, T. H., Jr.; Harrison, R. J. *J. Chem. Phys.* **1992**, *96*, 6796.

(27) (a) Papajak, E.; Truhlar, D. G. *J. Chem. Theor. Comput.* **2011**, *7*, 10. (b) Papajak, E.; Truhlar, D. G. *J. Chem. Theor. Comput.* **2010**, *6*, 597.
(28) Weigend, F.; Ahlrichs, R. *Phys. Chem. Chem. Phys.* **2005**, *7*, 3297.
(29) Frisch, M. J.; Trucks, G. W.; Schlegel, H. B.; Scuseria, G. E.; Robb, M. A.; Cheeseman, J. R.; Scalmani, G.; Barone, V.; Mennucci, B.; Petersson, G. A.; et al. *Gaussian 09*, Revision A.02; Gaussian, Inc.: Wallingford, CT, 2009.
(30) (a) Frisch, M. J.; Trucks, G. W.; Schlegel, H. B.; Scuseria, G. E.; Robb, M. A.; Cheeseman, J. R.; Scalmani, G.; Barone, V.; Mennucci, B.; Petersson, G. et al. *Gaussian 03*, Revision E.01; Gaussian, Inc.: Wallingford, CT, 2003. (b) Zhao, Y.; Truhlar, D. G. *MN-GFM: Minnesota Gaussian Functional Module*, version 4.1; University of Minnesota: Minneapolis, MN, 2008.
(31) Werner, H.-J.; Knowles, P. J.; Manby, F. R.; Schütz, M.; Celani, P.; Knizia, G.; Korona, T.; Lindh, R., Mitrushenkov, A.; Rauhut, G.; et al. *Molpro*, 2010.1; University of Birmingham: Birmingham, 2010.
(32) Zhao, Y.; Truhlar, D. G. *MLGAUSS* program, version 2.0; University of Minnesota: Minneapolis, 2007.
(33) Alecu, I. M.; Zheng, J.; Zhao, Y.; Truhlar, D. G. *J. Chem. Theor. Comput.* **2010**, *6*, 2872.
(34) Tishchenko, O.; Higashi, M.; Albu, T. V.; Corchado, J. C.; Kim, Y.; Villà, J.; Xing, J.; Lin, H.; Truhlar, D. G. *MCSI* computer program, version 2010; University of Minnesota: Minneapolis, 2010.
(35) Albu, T. V.; Tishchenko, O.; Corchado, J. C.; Kim, Y.; Jordi Villà, Villà, J.; Xing, J.; Lin, H.; Higashi, M.; Truhlar, D. G. *MC-TINKERATE* computer program, version 2010; University of Minnesota: Minneapolis, 2010.
(36) Garcia-Viloca, M.; Gao, J.; Karplus, M.; Truhlar, D. G. *Science* **2004**, *303*, 186.
(37) Albu, T. V.; Corchado, J. C.; Truhlar, D. G. *J. Phys. Chem. A* **2001**, *105*, 8465.
(38) Tishchenko, O.; Truhlar, D. G. *J. Chem. Theor. Comput.* **2009**, *5*, 1454.
(39) Lin, H.; Zhao, Y.; Tishchenko, O.; Truhlar, D. G. *J. Chem. Theory Comput.* **2006**, *2*, 1237.
(40) Kim, K. H.; Kim, Y. *J. Chem. Phys.* **2004**, *120*, 623.
(41) Allinger, N. L.; Yuh, Y. H.; Lii, J. H. *J. Am. Chem. Soc.* **1989**, *111*, 8551.
(42) Lii, J. H.; Allinger, N. L. *J. Am. Chem. Soc.* **1989**, *111*, 8566.
(43) Lii, J. H.; Allinger, N. L. *J. Am. Chem. Soc.* **1989**, *111*, 8576.
(44) Hornback, J. M. *Organic Chemistry*, 2nd ed.; Brooks/Cole: Pacific Grove, CA, 2005; p 91.
(45) Truhlar, D. G.; Gordon, M. S. *Science* **1990**, *249*, 491.
(46) Truhlar, D. G.; Brown, F. B.; Steckler, R.; A. Isaacson, D. In *The Theory of Chemical Reaction Dynamics*; Clary, D. C., Ed.; Reidel, D.: Dordrecht, Holland, 1986; pp 285−329.
(47) Zheng, J.; Truhlar, D. G. *Phys. Chem. Chem. Phys.* **2010**, *12*, 7782.
(48) Zheng, J.; Zhang, S.; Lynch, B. J.; Corchado, J. C.; Chuang, Y.-Y.; Fast, P. L.; Hu, W.-P.; Liu, Y. -P.; Lynch, G. C.; Nguyen, K. A.; et al. *POLYRATE*, version 2010-A; University of Minnesota: Minneapolis, 2010.